ISSN 1674-1056
http://cpb.iphy.ac.cn
http://iopscience.iop.org/cpb
中国物理 B
Chinese Physics
中国物理
Chinese Physics B

Energetic few-cycle pulse compression in gas-filled hollow core fiber with concentric phase mask

Yu Zhao(赵钰), Zhi-Yuan Huang(黄志远), Rui-Rui Zhao(赵睿睿), Ding Wang(王丁), Yu-Xin Leng(冷雨欣)

Citation: Chin. Phys. B . 2019, 28(6): 064207. **doi:** 10.1088/1674-1056/28/6/064207
Journal homepage: http://cpb.iphy.ac.cn; http://iopscience.iop.org/cpb

What follows is a list of articles you may be interested in

Generation of few-cycle radially-polarized infrared pulses in a gas-filled hollow-core fiber

Rui-Rui Zhao(赵睿睿), Zhi-Yuan Huang(黄志远), Ding Wang(王丁), Yu Zhao(赵钰), Yu-Xin Leng(冷雨欣), Ru-Xin Li(李儒新)
Chin. Phys. B . 2018, 27(10): 104204. **doi:** 10.1088/1674-1056/27/10/104204

Self-compression of 1.8-μm pulses in gas-filled hollow-core fibers

Rui-Rui Zhao(赵睿睿), Ding Wang(王丁), Yu Zhao(赵钰), Yu-Xin Leng(冷雨欣), Ru-Xin Li(李儒新)
Chin. Phys. B . 2017, 26(10): 104206. **doi:** 10.1088/1674-1056/26/10/104206

Spatiotemporal propagation dynamics of intense optical pulses in loosely confined gas-filled hollow-core fibers

Rui-rui Zhao(赵睿睿), Ding Wang(王丁), Zhi-yuan Huang(黄志远), Yu-xin Leng(冷雨欣), Ru-xin Li(李儒新)
Chin. Phys. B . 2017, 26(1): 014208. **doi:** 10.1088/1674-1056/26/1/014208

Nonlinear compression of picosecond chirped pulse from thin-disk amplifier system through a gas-filled hollow-core fiber

Jun Lu(陆俊), Zhi-Yuan Huang(黄志远), Ding Wang(王丁), Yi Xu(许毅), Yan-Qi Liu(刘彦祺), Xiao-Yang Guo(郭晓杨), Wen-Kai Li(黎文开), Fen-Xiang Wu(吴分翔), Zheng-Zheng Liu(刘征征), Yu-Xin Leng(冷雨欣)
Chin. Phys. B . 2016, 25(12): 124207. **doi:** 10.1088/1674-1056/25/12/124207

Generation of few-cycle laser pulses: Comparison between atomic and molecular gases in a hollow-core fiber

Zhi-Yuan Huang(黄志远), Ye Dai(戴晔), Rui-Rui Zhao(赵睿睿), Ding Wang(王丁), Yu-Xin Leng(冷雨欣)
Chin. Phys. B . 2016, 25(7): 074205. **doi:** 10.1088/1674-1056/25/7/074205

Energetic few-cycle pulse compression in gas-filled hollow core fiber with concentric phase mask*

Yu Zhao(赵钰)[1,2], Zhi-Yuan Huang(黄志远)[1,2], Rui-Rui Zhao(赵睿睿)[1,2], Ding Wang(王丁)[1,†], and Yu-Xin Leng(冷雨欣)[1,‡]

[1] *State Key Laboratory of High Field Laser Physics, Shanghai Institute of Optics and Fine Mechanics, Chinese Academy of Sciences, Shanghai* 201800, *China*
[2] *Center of Materials Science and Optoelectronics Engineering, University of Chinese Academy of Sciences, Beijing* 100049, *China*

(Received 21 February 2019; revised manuscript received 28 March 2019; published online 29 May 2019)

The compression of high-energy, linearly polarized pulses in a gas-filled hollow core fiber (HCF) by using a concentric phase mask is studied theoretically. Simulation results indicate that using a properly designed concentric phase mask, a 40-fs input pulse centered at 800 nm with energy up to 10.0 mJ can be compressed to a full width at half maximum (FWHM) of less than 5 fs after propagating through a neon-filled HCF with a length of 1 m and diameter of 500 μm with a transmission efficiency of 67%, which is significantly higher than that without a concentric phase mask. Pulses with energy up to 20.0 mJ can also be efficiently compressed to less than 10 fs with the concentric phase mask. The higher efficiency due to the concentric phase mask can be attributed to the redistribution of the transverse intensity profile, which reduces the effect of ionization. The proposed method exhibits great potential for generating few-cycle laser pulse sources with high energy by the HCF compressor.

Keywords: pulse compression, hollow-core fiber, phase mask

PACS: 42.65.–k, 42.81.Qb, 42.79.Ci **DOI:** 10.1088/1674-1056/28/6/064207

1. Introduction

Over the past decades, few-cycle laser sources with high energy have been extensively studied. These are powerful tools for investigating of high field laser and plasma physics, such as high-order harmonic generation,[1–3] attosecond physics,[4–7] and laser particle acceleration.[8–11] Owing to the development of the chirped pulse amplification (CPA) technique,[12] Ti:Sapphire lasers have been widely used as sources of stable, energetic, and ultrashort pulses for several experiments. However, the output durations of the pulses are limited to tens of fs (at a central wavelength of 800 nm) due to the finite bandwidth of the gain medium. To achieve shorter durations, several schemes have been proposed and demonstrated, such as optical parametric CPA (OPCPA),[13–15] thin-film compressors (TFC),[16,17] femtosecond filamentation in noble gas,[18–20] and the hollow core fiber (HCF) compressor filled with noble gas.[21–24] Of these methods, the HCF compressor is the most widespread in the laboratory practice in the world. Compared with the pulse compression using bulk materials or traditional fibers, the HCF compressor can improve the output energy to the mJ level and the beam quality while preserving the few-cycle pulse duration after the pulse compression.[25] The fundamental principle of the HCF compressor is simple. First, energetic laser pulses are coupled into the HCF filled with noble gas. During the propagation in the HCF, the spectrum of the input pulses is broadened by self-phase modulation (SPM). Then, the output pulses from the HCF are collimated and directed to chirped mirrors for compensation.[26,27] While this method is an established technique, the energy of the input pulse is limited to several mJ to reduce the ionization effects at the inlet of the HCF, which deteriorates the transmission efficiency and the beam profile. Next, a pressure gradient hollow waveguide compressor is used to generate ultra-intense few-cycle linearly polarized (LP) pulses in the experiment.[28,29] Bohman *et al.*[28] demonstrated the generation of 5.0-fs, 5.0-mJ pulses at a repetition rate of 1 kHz with an energy transmission efficiency lower than 50%. Cardin *et al.*[29] suggested that by employing pulse compression with a stretched HCF, 2-cycle pulses at 1.8 μm (12 fs) carrying pulse energy of 5.0 mJ at a repetition rate of 100 Hz can be obtained for input pulses with energy of 11.0 mJ to propagate in a 3-m-long argon-filled HCF. The HCF compressor with static pressure is also a general method to generate intense few-cycle laser sources in simulation and experiment. Dutin *et al.*[30] recommended the generation of 11.4-fs pulses with total energy of 13.7 mJ, starting from 40-fs, 70-mJ input pulses, through a capillary filled with helium, with a pressure in the capillary being less than 8 mbar (1 bar = 10^5 Pa). Moreover, Chen *et al.*[31] reported the generation of 4.3-fs 1.0-mJ pulses at 1 kHz, using an HCF

*Project supported by the National Natural Science Foundation of China (Grant No. 61521093), the Strategic Priority Research Program of the Chinese Academy of Sciences (Grant No. XDB1603), the International Science and Technology Cooperation Program of China (Grant No. 2016YFE0119300), and the Program of Shanghai Academic/Technology Research Leader, China (Grant No. 18XD1404200).

†Corresponding author. E-mail: wangding@siom.ac.cn
‡Corresponding author. E-mail: lengyuxin@mail.siom.ac.cn

© 2019 Chinese Physical Society and IOP Publishing Ltd

compressor seeded with circularly polarized (CP) laser pulses, while the generation of high-power carrier-envelope phase stabilized sub-1.5 cycle CP pulses at 1.8 μm was reported by Song *et al.*[32] On the one hand, Chen *et al.* observed energy throughput up to 30% higher than that of LP input pulses, that is, the transmission efficiency of the CP pulses after the HCF is higher than that of the LP pulses under the identical initial conditions. On the other hand, the generated CP laser pulses are usually transformed into LP pulses by a quarter wave plate in experiment. However, the CP pulses are limited by the finite bandwidth of the wave plate, therefore compared with CP pulses, the LP pulses are widely used in optical experiments. In addition to LP and CP pulses, the few-cycle radially polarized (RP) pulses with energy of a few mJ in experiment[33] and simulation[34] have been achieved by use of a pressure gradient hollow-waveguide compressor. The output pulses can be compressed to 8 fs experimentally and to 6 fs (FWHM) in simulation, with transmission efficiencies of 60% and 85%, respectively.

In 2009, using a single-step phase plate, Fu *et al.*[35] found that the input pulses with higher energy propagating in air can generate a single filament and extended filaments. Rohwetter *et al.*[36] suggested that a smooth phase mask can control multiple filamentation of laser in air and confirmed this experimentally. Liu *et al.*[37] achieved accurately controllable multiple femtosecond filamentation in air, by employing a combination of half-wave phase plates. The aim of these methods is first to change the optical field distribution of the input pulses by modulating the phase, then reducing the peak intensity of the input pulses and weakening the plasma defocusing effect, in the end increasing the transmission efficiency after pulse propagation in HCF. Based on these studies, the HCF compressor with a concentric phase mask is expected to deliver more energetic ultrashort pulses with higher transmission efficiency. In the near future, this method can also be applied to the generation of ultra-intense few-cycle CP laser pulses.

In this paper, we theoretically investigate the effect of a concentric phase mask on the dynamic propagation and generation of high-energy few-cycle pulses through a gas-filled HCF. It is shown that by using a properly designed concentric phase mask, a 40-fs input pulse centered at 800 nm with energy up to 10.0 mJ can be compressed to less than 5 fs after propagating through a neon-filled HCF with a length of 1 m and diameter of 500 μm. The transmission efficiency of 67% is significantly higher than that without a concentric phase mask. Pulses with energy up to 20.0 mJ can also be efficiently compressed to less than 10 fs, with the concentric phase mask used. The advantage of using a concentric phase mask can be attributed to the redistribution of the transverse intensity profile, which reduces the effect of ionization. Thus, this method is suitable for generating the few-cycle and high-energy pulses. The remainder of the paper is organized as follows. In Section 2 the theoretical model used in this work is described. In Section 3 the simulation results are presented in the case with using the concentric phase mask, and also compared with the results in the case without using the concentric phase mask after the pulses have propagated through the HCF. Finally, some conclusions are drawn from the present study in Section 4.

2. Theoretical model and method

We assume that the equation of pulse propagation in the atomic gas-filled HCF corresponds to a cylindrical symmetric model. Thus, the propagation dynamics of LP pulses in the HCF can be described by the generalized unidirectional pulse propagation equations with lossy boundary conditions (gUPPE-b)[38–40] as follows:

$$\partial_z E(z,r,\omega) = \mathrm{i}\left(\sqrt{\hat{L}''} - \frac{\omega}{v_\mathrm{g}}\right)E(z,r,\omega) + \frac{\omega}{2\beta c^2}\left[\mathrm{i}\omega\frac{P(z,r,\omega)}{\varepsilon_0} - \frac{j(z,r,\omega)}{\varepsilon_0}\right], \quad (1)$$

where the pulse envelope $E(z,r,\omega)$ is the optical field distribution in the frequency domain, $\hat{L}''$ describes the dispersion and diffraction effect, $\beta = \omega n(\omega)/c$ is the frequency-dependent wavenumber, v_g is the group velocity of the propagating pulse, $P(z,r,\omega)$ and $j(z,r,\omega)$ are the nonlinear polarizations related to the bounded and free electrons, respectively, ε_0 is the vacuum permittivity, ω is the angular frequency, and c is the speed of light. For the cubic Kerr effect, the nonlinear polarization in the time domain is $\boldsymbol{P}(t) = \chi^{(3)}_{1111}|\boldsymbol{E}(t)|^2\boldsymbol{E}(t)$,[41] where $\chi^{(3)}_{1111}$ is the third-order nonlinear susceptibility tensor component, and $\boldsymbol{E}(t)$ is the vectorial expression of the optical field distribution in the time domain.

The gas ionization effect is described by $j(t)/\varepsilon_0 = cn_0\eta W(I)U_\mathrm{i}(\rho_\mathrm{nt}-\rho)E/I$, where $W(I)$ is the ionization rate calculated according to the Perelomov–Popov–Terent'ev model,[42] ρ is the electron density, ρ_nt is the neutral density of gas, I is the pulse intensity envelope, and U_i is the ionization potential. The plasma effect can be described by

$$\frac{j(\omega)}{\varepsilon_0} = \frac{\tau_\mathrm{c}(1+i\omega\tau_\mathrm{c})}{1+\omega^2\tau_\mathrm{c}^2}\frac{e^2}{\varepsilon_0 m_\mathrm{e}}\boldsymbol{FFT}[\rho E],$$

where e denotes the electron charge, m_e is the mass, and τ_c is the collision time. Assuming that the ionized electrons are created at rest, the evolution of electron density ρ is given by

$$\partial_t\rho = W(I)(\rho_\mathrm{nt}-\rho) + \frac{\sigma\rho I}{U_\mathrm{i}}, \quad (2)$$

where σ is the cross section of impact ionization.

The concentric phase mask consists of two parts and it is made of BK7 optical glass as shown in Fig. 1. The central part of the concentric phase mask (region 1 in Fig. 1) is thinned by

wet etching to produce a π -phase shift of the 800-nm working wavelength. The duty cycle of the concentric phase mask is the ratio of the radius of region 1 to the radius of the entire concentric phase mask, *i.e.*, $n = r_1/r_2.\phi_1$ represents the phase retardation of the central part of the concentric phase mask, *i.e.*, the birefringent half-wave plate, and ϕ_2 is the phase retardation of the circular ring of the concentric phase mask. Moreover, the thickness of region 2 is the same as that of region 1. In our simulation, $\phi_1 = \pi$, $\phi_2 = 0$ and $0 \le n \le 1$.

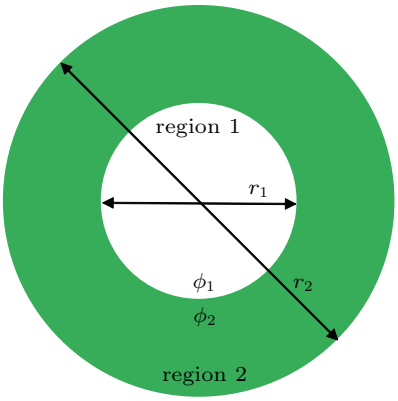


Fig. 1. Schematic diagram of concentric phase mask, where Region 1 represents birefringent half-wave plate.

According to Ref. [43], there is a boundary condition for input pulses transmitted through the HCF: the field at the intersection between the fiber core and fiber clad is $E_{\text{intersection}} = (E_{\text{TE}} + E_{\text{TM}})/2$, where $E_{\text{TE}} = (4E_1 - E_2)/(3 - 2\text{i}k_{\text{clad}}\Delta r)$ and $E_{\text{TM}} = (4E_1 - E_2)/(3 - 2\text{i}k_{\text{clad}}\Delta r/n_{\text{clad}}^2)$, with E_1 and E_2 being the fields at distances of Δr and $2{\cdot}\Delta r$ from the boundary of the hollow core, respectively, k_{clad} the wavenumber, and n_{clad} the refractive index of the fiber clad. After the input pulses are incident on the concentric phase mask and then focused on the entrance of a neon-filled HCF, the envelope of the initial input pulses can be described by

$$E(z=0,r,t) = E(z=0,r)\exp\left(-\frac{t^2}{2T_0^2}\right), \tag{3}$$

$$E(z=0,r) = E(r)f(r), \tag{4}$$

$$E(r) = E_1(r) + E_2(r), \tag{5}$$

$$f(r) = \exp\left(\frac{\text{i}k_0 r^2}{2f}\right)\frac{\exp(\text{i}k_0 f)}{\text{i}\lambda_0 f}, \tag{6}$$

$$E_1(r) = FFT\left\{\left(E_0\exp\left(-\frac{r^2}{\omega_0^2}\right), 0 \le r \le n\omega_0\right)\exp(\text{i}\phi_1)\right\}, \tag{7}$$

$$E_2(r) = FFT\left\{\left(E_0\exp\left(-\frac{r^2}{\omega_0^2}\right), n\omega_0 \le r \le 2\omega_0\right)\exp(\text{i}\phi_2)\right\}, \tag{8}$$

where E_0, ω_0, T_0, k_0, λ_0 , and f represent the amplitude, the beam waist, the duration, the vacuum wavenumber, the central wavelength of the initial input pulse, and the focal length of the convex lens, respectively. The distance from the central axis is denoted by r, and a represents the radius of the HCF. However, the analytical solution of Eq. (3) cannot be obtained by calculating the fast Fourier transform in Eqs. (7) and (8). Thus, we use several numerical fitting solutions with different duty cycles, such as

$$I(z=0,r,t) = |E(z=0,r,t)|^2 = I_{\text{peak}}F(r)\exp\left(-\frac{t^2}{T_0^2}\right), \tag{9}$$

$$I_{\text{peak}} = \frac{E_{\text{in}}}{2\pi^{3/2}T_0\int_0^\infty F(r)r\text{d}r}, \tag{10}$$

$$F(r) = \sum_{n=1}^{N} a_n \exp\left(-\frac{(r-b_n)^2}{c_n^2}\right), \tag{11}$$

where $I_{\text{peak}}, E_{\text{in}}, \int_0^\infty F(r)r\text{d}r$ denote the peak intensity, the initial energy, and the spot area of input pulses, respectively, and N denotes the number of Gaussian polynomials. The specified values of a_n, b_n, c_n are listed in Table 1. The root mean square error of the fitting solutions is smaller than 0.1% for all numerical fitting solutions.

Table 1. Specific numerical values in Eq. (11).

	$n = 0.4$	$n = 0.5$	$n = 0.6$	$n = 0.8$
a_1	1.011	1.488	0.8875	1.095
b_1	3.355	104.5	111.2	1.886
c_1	57.2	45.86	30.1	95.67
a_2	0.1589	0.9574	0.9097	30
b_2	193.4	−115.8	−105.1	−141.1
c_2	46.25	38.14	30.74	6.553×10^4
a_3	0.1591	0.7679	0.2387	0.0004943
b_3	−186.8	4.956	142.9	−2013
c_3	46.34	40.92	22.08	801.7
a_4	0.1476	2.27	0.2651	−0.0005559
b_4	260.8	138	−137.7	2.9×10^8
c_4	75.35	51	22.92	-4.9×10^8
a_5	0.1472	0.1853	0.3599	0.002041
b_5	−254.2	−150.3	78.45	−404.6
c_5	75.46	26.07	25.78	807.3
a_6	0.008165	−2.398	0.2927	0.00205
b_6	607.9	126.2	−72.09	404.7
c_6	106.9	67.7	24.67	807.3
a_7		−0.1662	0.156	−0.0005501
b_7		−51.07	238	1237
c_7		28.17	32.08	843.3
a_8		0.2016	0.156	0.0004882
b_8		206.9	−234.2	2013
c_8		67.5	32.04	801.6

Figure 2 shows the normalized spatial and radial intensity distributions of the input 40 fs pulses with energy in a range of 5.0 mJ–20.0 mJ before they are coupled into the HCF. The spatial spot in Fig. 2(a) and the curve in Fig. 2(b) correspond to the light emitted by a Ti:Sapphire laser device. Figures 2(c) and 2(d) show the intensity distribution at the focus for the LP Gaussian laser pulses in Figs. 2(a) and 2(b) after a focal lens

(convex lens). The last row in Fig. 2 denotes the intensity distribution for the LP Gaussian laser pulses in Figs. 2(a) and 2(b) after a concentric phase mask and a focal lens.

In this paper, $v = w_0/a$ (w_0 is the spot size or waist radius of the input pulse, a is the inner radius of the HCF) is not the most important parameter. In our simulation, the spot size at the inlet of the HCF is set to be approximately 330 μm, which possibly does not satisfy the optimal coupling condition for the input pulses after the phase mask. However, the waist radius is implicitly included in Gaussian polynomial in Eq. (11); therefore, it cannot be calculated directly by Eqs. (9)–(11). The real spot size of the input pulses with the concentric phase mask needs to be adjusted by the focal length of the convex lens used in the experiment. Thus, as shown in Fig. 2(f), the spot size of the input pulses after the phase mask is also defined as the distance from the maximum intensity down to the $1/e^2$ of the maximum intensity (as indicated by the length of the green dash line in Fig. 2(f)). Using a single-step phase plate, Fu *et al.*[35] experimentally found that the input pulses with higher energy propagating in air can generate a single filament. Therefore, the input pulses after a single-step phase plate are mostly coupled into the EH_{11} mode. Similarly, the method is also applied to the pulse compression in the HCF; therefore the input LP pulses after the phase mask are coupled mostly into the EH_{11} mode as well in the HCF. The simulation results in this study suggest that the output energy of the pulses after the phase mask is higher than that of the pulses without phase mask, and the input pulses without the phase mask are mostly coupled into the EH_{11} mode in the HCF. Therefore, it is recommended that the major energy of the input pulses with phase mask is coupled into the EH_{11} mode in HCF. Then the fundamental idea is to compare the compression results between different duty cycles. Considering that the aim of this study is to introduce a convenient and novel method to obtain ultrashort pulses with high energy and low loss after propagating in the HCF, thus the duty cycle of the concentric phase mask is the most significant variable. Moreover, according to Eq. (10) the peak intensities of the input pulses in Figs. 2(c) and 2(e) are increased up to 3.23×10^{14} W/cm^2 and 2.15×10^{14} W/cm^2, respectively.

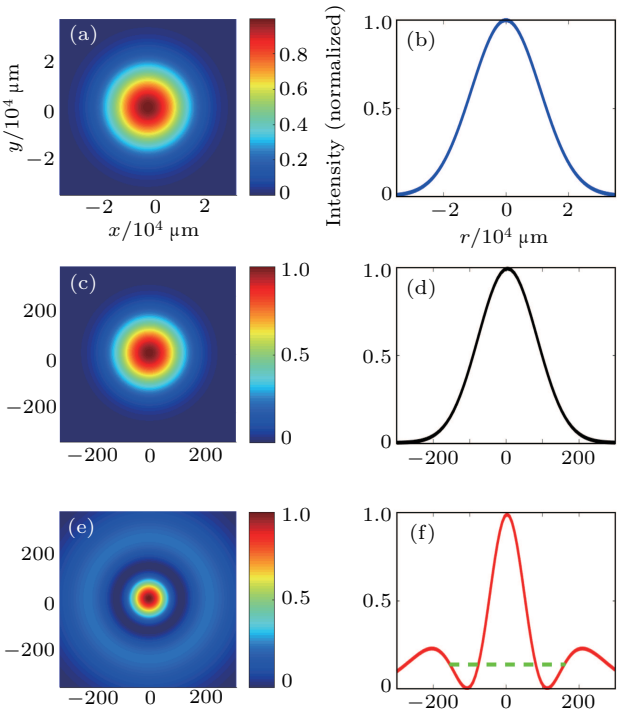


Fig. 2. (a), (c), (e) Normalized spatial intensity distributions and (b), (d), and (e) radial intensity distributions of input pulses before propagating in HCF. Panes (a) and (b) show intensity profiles for LP Gaussian laser pulses, panels (c) and (d) show intensity profiles of incident focused LP Gaussian laser pulses after convex lens, and panels (e) and (f) show incident focal laser pulses after concentric phase mask and convex lens with duty cycle of 0.4.

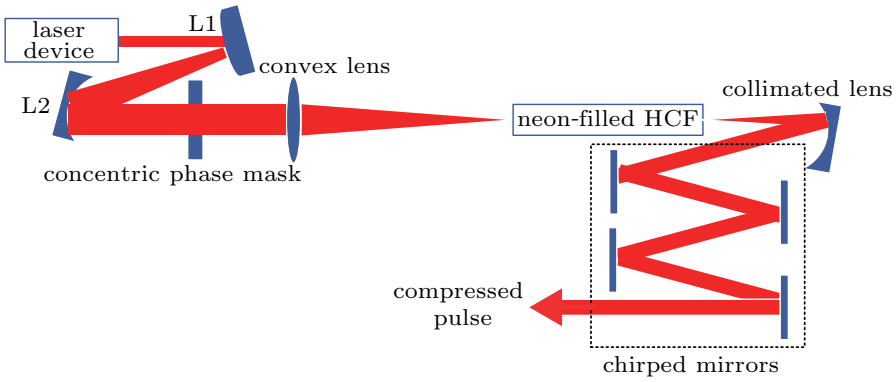


Fig. 3. Experimental setup for few-cycle pulse compression in neon-filled HCF with concentric phase mask. L1 and L2 represent convex and concave reflecting mirror, respectively. Combination of L1 and L2 is telescope.

As shown in Fig. 3, the initial pulse is first incident on a telescope system for beam expanding, then goes via a concentric phase mask and is focused by a focal lens that is computed by Eqs. (9)–(11), after that, coupled into a gas-filled hollow-core fiber (HCF) for spectral broadening, which is simulated through the integration of the propagation equation (1). Then, the pulse is collimated and reflected on several chirped mirrors for chirp compensation; as a result, the pulse is compressed. The chirped mirrors are carefully designed to induce a fixed second-order chirp and a third-order chirp per reflection in the

pulse. Therefore, the process of pulse compression can be simulated by simply adding a phase term to the pulse, as follows:

$$E_{\text{compress}}(r,\omega) = E_{\text{output}}(r,\omega)\exp(\mathrm{i}d_{\text{GDD}}(\omega-\omega_0)^2/2!) \times \exp(\mathrm{i}d_{\text{TOD}}(\omega-\omega_0)^3/3!), \quad (12)$$

where $E_{\text{output}}(r,\omega)$ describes the pulse after propagating in the HCF and before reflecting on the chirped mirrors, $E_{\text{compress}}(r,\omega)$ describes the pulse after the reflecting on the chirped mirrors, which leads to the total group delay dispersion (GDD) of d_{GDD} and the third-order dispersion (TOD) of d_{TOD}, while ω_0 is the central angular frequency.

3. Results and discussion

The numerical values in this section correspond to an initial Fourier transform-limited pulse of 40 fs (FWHM) centered at 800 nm and input pulse energy of 10.0 mJ, while the length and inner diameter of the neon-filled HCF are 1 m and 500 μm, respectively. Because the gas pressure can affect the energy loss, dispersion and nonlinear process, the pressure of neon is optimized under different duty cycles, thus the pressure values in the HCF are 100 mbar, 1400 mbar, 800 mbar, 600 mbar, and 1000 mbar, of which the corresponding duty cycles of the concentric phase mask are 0.0, 0.4, 0.5, 0.6, and 0.8. Firstly, we compare the energy transmissions for different duty cycles of the concentric phase mask under the respective optimal pressure as shown in Fig. 4. The energy transmission exceeds 65% when the duty cycle of the concentric phase mask is 0.4, while the energy transmission decreases to 53.5% after the pulses have propagated through the HCF without concentric phase mask. For propagation distances less than 20 cm, the energy transmissions of $n = 0.4$, 0.5, 0.6, and 0.8 drop slowly due to the relatively weak ionization. However, because the peak plasma intensity is strong due to the relatively powerful peak intensity of the input pulses, a sharper decline occurs when the duty cycle of the concentric phase mask is 0. For distance greater than 20 cm, where the leakage loss of the HCF and the loss resulting from the plasma defocusing effect reduce the peak power of the pulses, the amount of plasma generated by the ionization effects also decreases. Thus, the lines shown in Fig. 4 become smooth. The phenomenon shown in Fig. 4 results from the input pulses after the concentric phase mask, which can change the optical field distribution, and thus attenuating the peak intensity of the input LP pulses as shown in Fig. 2.

As shown in Fig. 5, the width of compressed pulses without concentric phase mask is 8.2 fs, while the widths of compressed pulses after the concentric phase mask of duty cycles of 0.4, 0.5, 0.6, and 0.8 are 4.9 fs, 7.5 fs, 9.9 fs, and 7.0 fs, respectively. Thus the HCF compressor with concentric phase mask is easier to generate energetic few-cycle pulses than without phase mask. It should be noted that the chirp, induced by the propagation after the HCF and the chamber window, is not considered. Thus, the optimal chirp compensation is different from that in experiment. Particularly, the output energy exceeds 6.0 mJ after the pulse has propagated through the HCF, for the duty cycles of concentric phase masks are 0.4 and 0.6. From Fig. 6, it can be seen that the spatial distributions of compressed pulses with concentric phase mask are closer to the fiber core and the spot size becomes smaller than without phase mask. When the concentric phase mask is used, the energy loss decreases after pulse propagating in HCF.

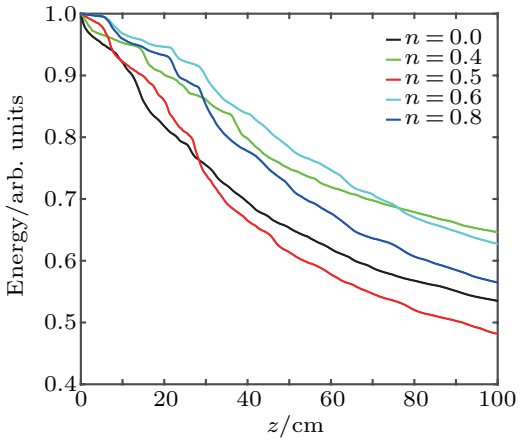


Fig. 4. Energy transmissions with different duty cycles of concentric phase mask during input pulses propagating in HCF.

Figure 7 shows the spectrum of output pulses with and without using the concentric phase mask. The spectrum in Fig. 7(a) covers the range of 380 nm–900 nm, which is slightly broader than the spectrum after using the concentric phase mask. It can be seen that the SPM effect is important in the process of pulse propagation in the HCF, strongly affecting the output power spectra shown in Fig. 7. On the one hand, the spectrum becomes more nonuniform and splits into several parts along pulses propagating in the HCF; these phenomena are shown in Figs. 8 and 9. On the other hand, higher peak intensity induces a stronger blue-shift in the spectra of the input pulses without phase mask as shown in Figs. 7(a) and 8, than in the spectra of the input pulses with phase mask as shown in Figs. 7(b) and 9. As can be seen in Fig. 8, the spatio-spectral distribution is more nonuniform during the pulses propagating in the HCF, which is different from the counterpart shown in Fig. 9. The spectrum in Fig. 8 becomes more inhomogeneous at distances less than 60 cm, and becomes cleaner for distances greater than 60 cm. Moreover, the spatial spectral distribution of the input pulses without phase plate is closer to the cladding of HCF than that of the input pulses after phase

plate. Thus the concentric phase mask is able to reduce energy loss along pulses propagating in HCF as illustrated in Fig. 4.

In theory, the broader spectrum of pulses can support a narrower duration of compressed pulses; thus, the output pulses without concentric phase mask can be compressed easier by chirp compensation than those with using concentric phase mask. However, the energy transmission of the output pulses in the case without the concentric phase mask is significantly less than that in the case with the concentric phase mask. In general, the condition where the duty cycle of the concentric phase mask is 0.4 can be considered as the relatively optimal condition for high-energy pulse propagation and compression. In the following, we numerically examine and discuss the compression results, mainly for the HCF compressor with the concentric phase mask.

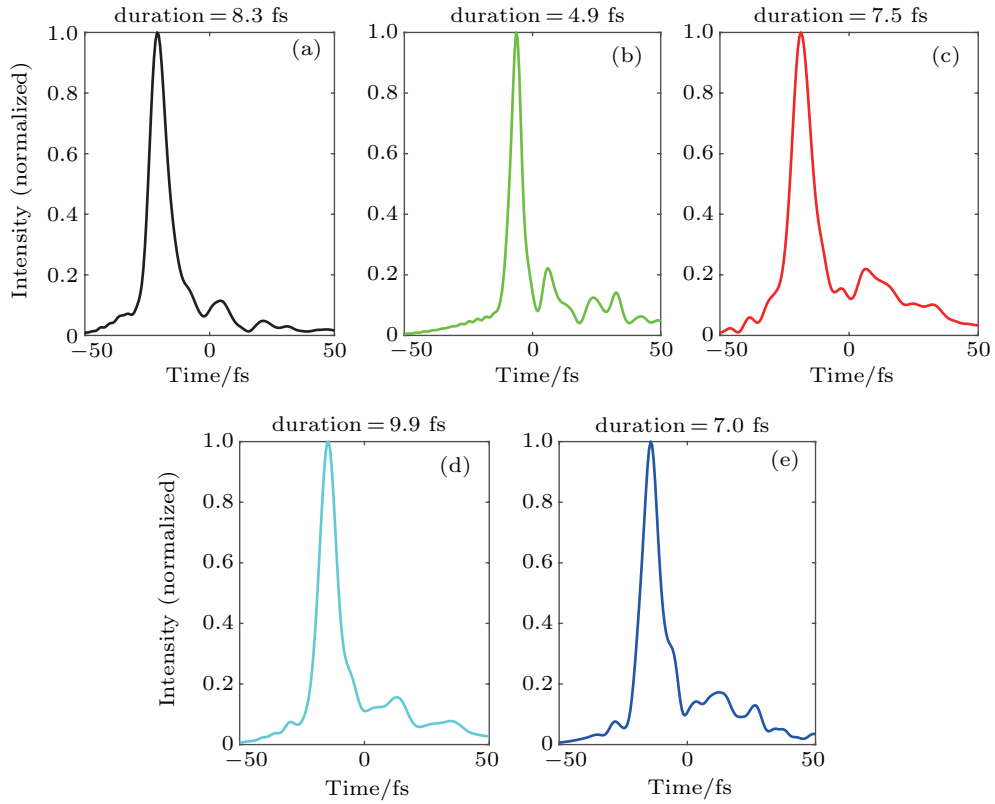


Fig. 5. Temporal power profiles of compressed pulses with and without concentric phase mask for input energy of 10.0 mJ: (a) without concentric phase mask, (b)–(e) with concentric phase mask under duty cycles of 0.4, 0.5, 0.6, and 0.8. (a)–(e) GDD compensations are −42.5, −38.0, −55.0, −41.0, and −49 fs^2, respectively, and TOD compensations are 0, 80, 0, 0, 50 fs^3.

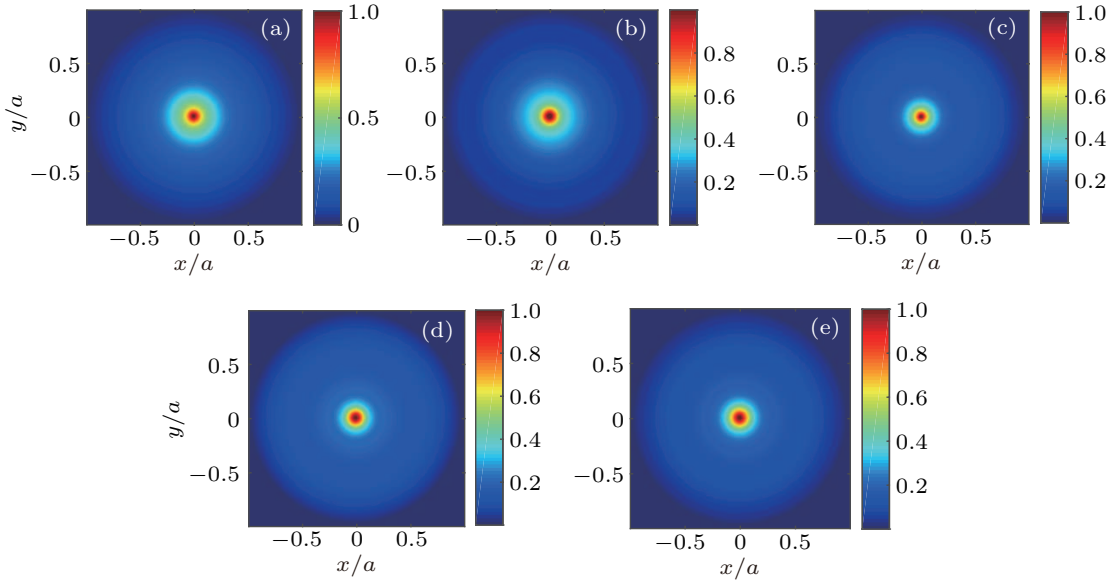


Fig. 6. Normalized spatial intensity profiles of compressed pulses: (a) compressed pulses without concentric phase mask and (b)–(e) compressed pulses with concentric phase mask under duty cycles of 0.4, 0.5, 0.6, and 0.8.

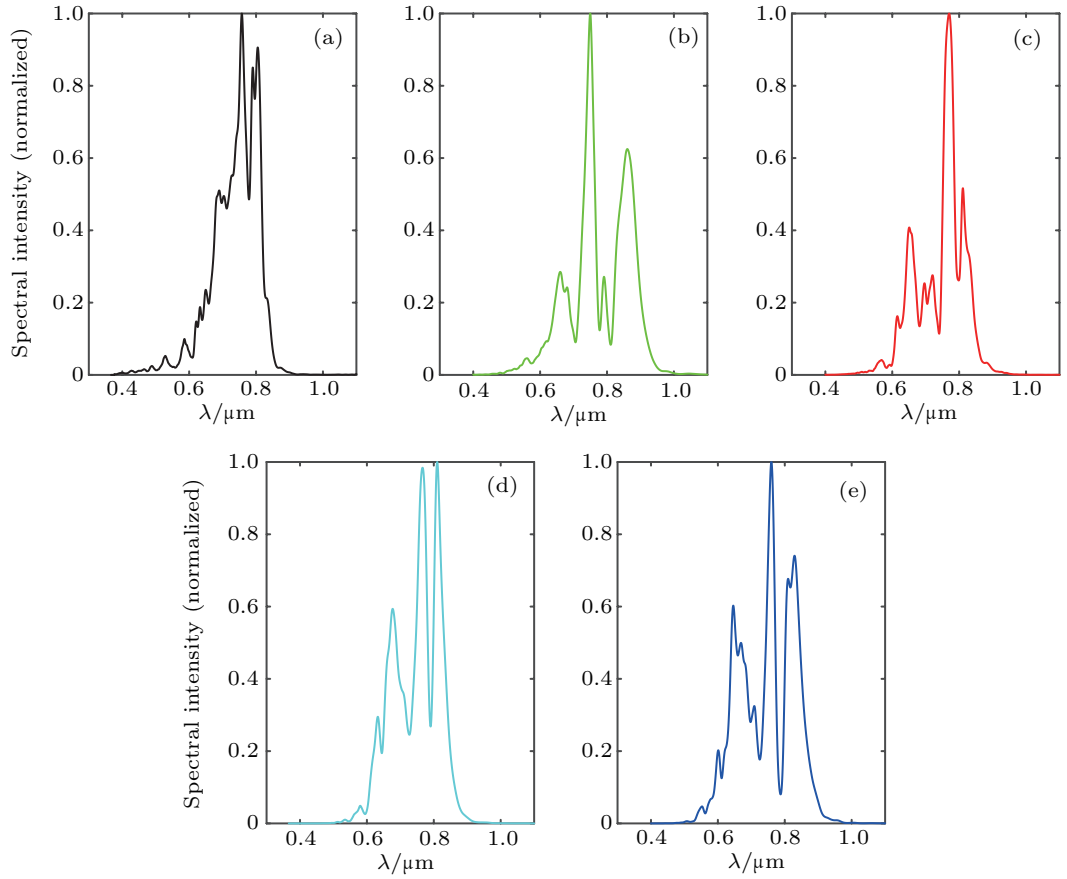


Fig. 7. Output power spectra of the input pulses passing through concentric phase mask of different duty cycles: (a) $n = 0$, (b) $n = 0.4$, (c) $n = 0.5$, (d) $n = 0.6$, and (e) $n = 0.8$.

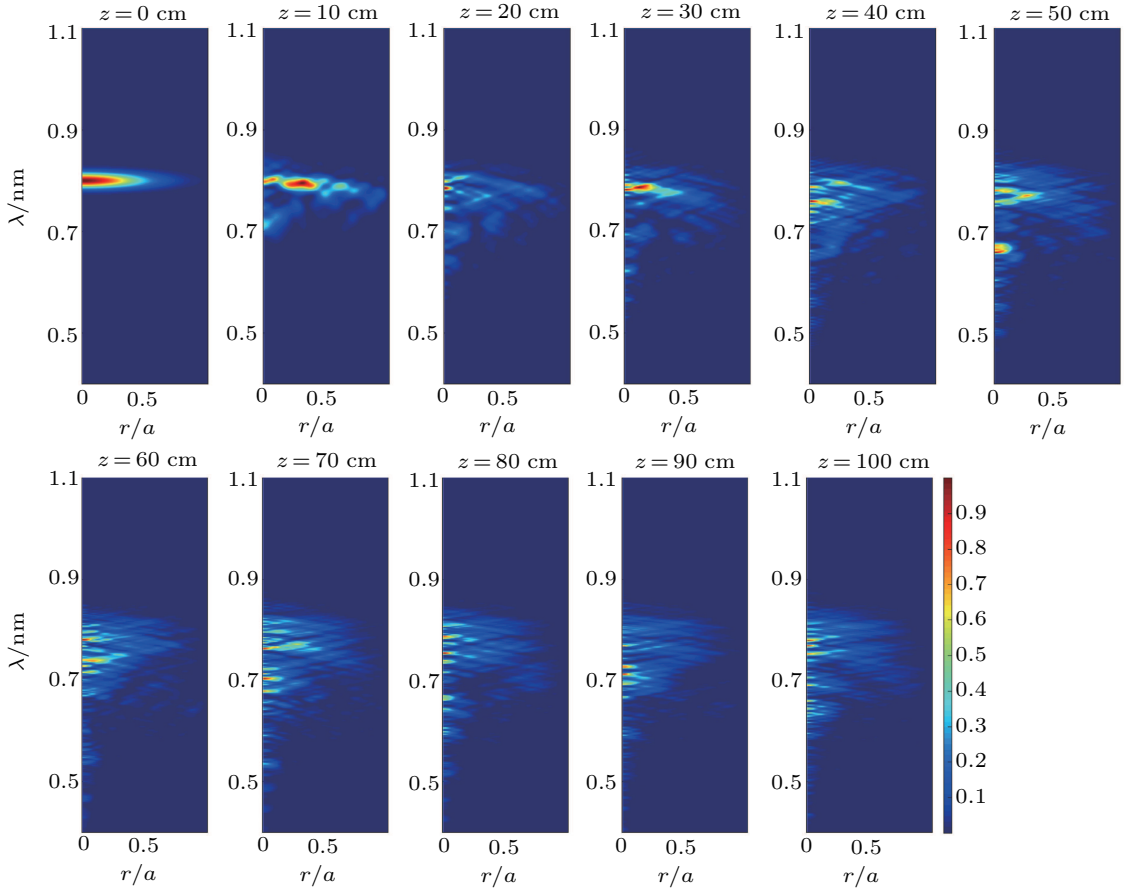


Fig. 8. Normalized spatio-spectral distributions along fiber axis z for input pulses without phase mask.

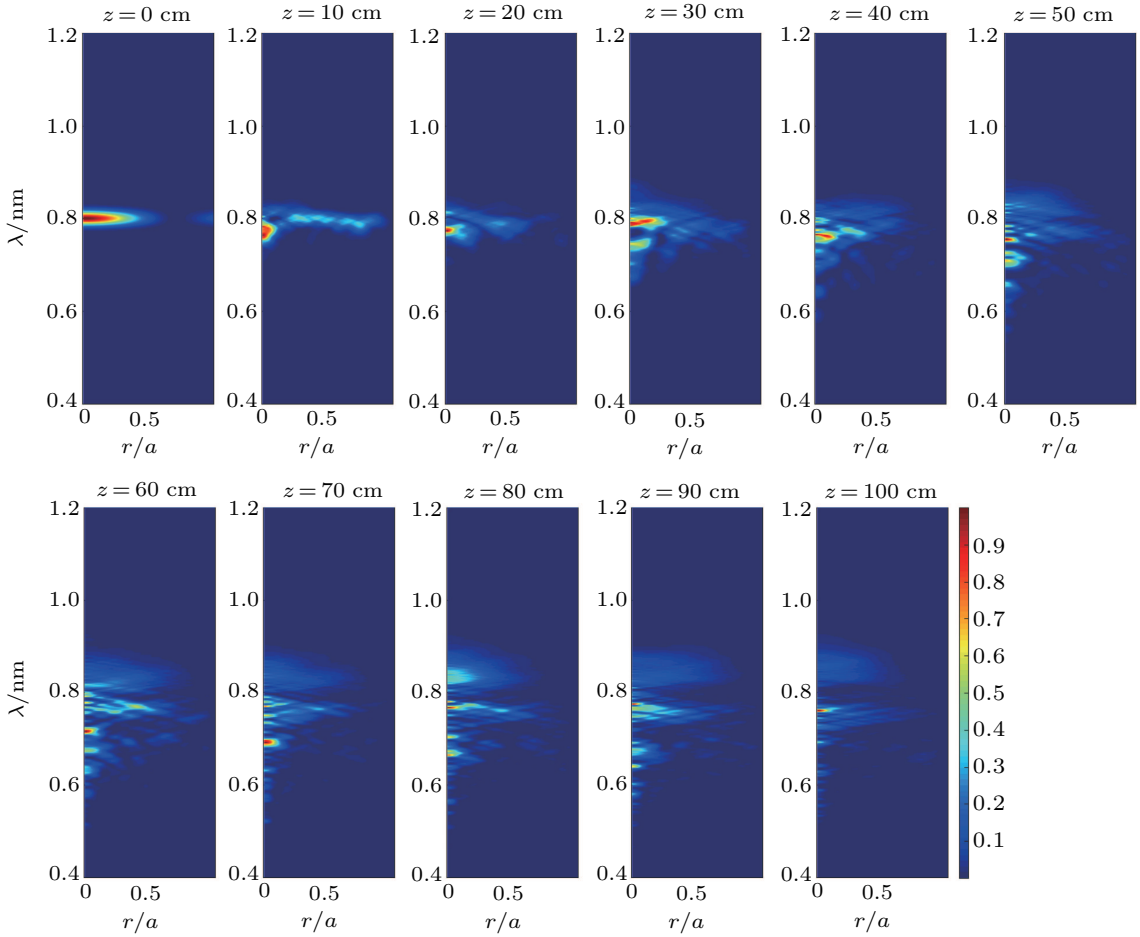


Fig. 9. Normalized spatio-spectral distributions along fiber axis z for input pulses with phase mask under duty cycle of 0.4.

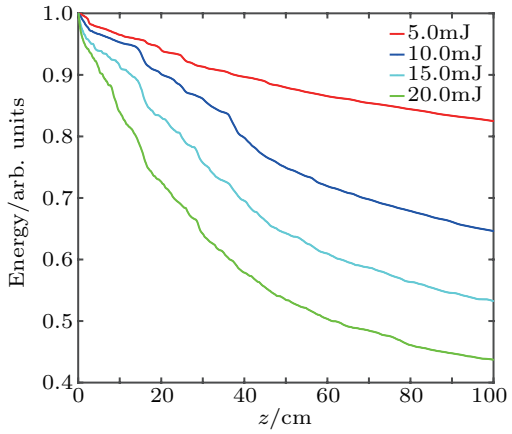


Fig. 10. Energy transmissions of input pulses during propagation in HCF with different input energy.

For a better understanding of the propagation characteristics of the input pulses after the concentric phase mask, we also simulate the input pulses of different energy under an appropriate pressure. The numerical values given in this section correspond to an initial Fourier transform-limited pulse of 40 fs (FWHM) centered at 800 nm with the initial energy in a range of 5.0 mJ–20.0 mJ. The length and diameter of the neon-filled HCF is 1 m and 500 μm, respectively. The pressures in the HCF are 3000 mbar, 1400 mbar, 600 mbar, and 300 mbar for a 0.4 duty cycle of the concentric phase mask. The energy transmissions shown in Fig. 10 are in a range of 83%–43% when the initial energy increases. It can be seen that the energy transmissions vary linearly with the propagation distance for less than initial energy of 10.0 mJ,

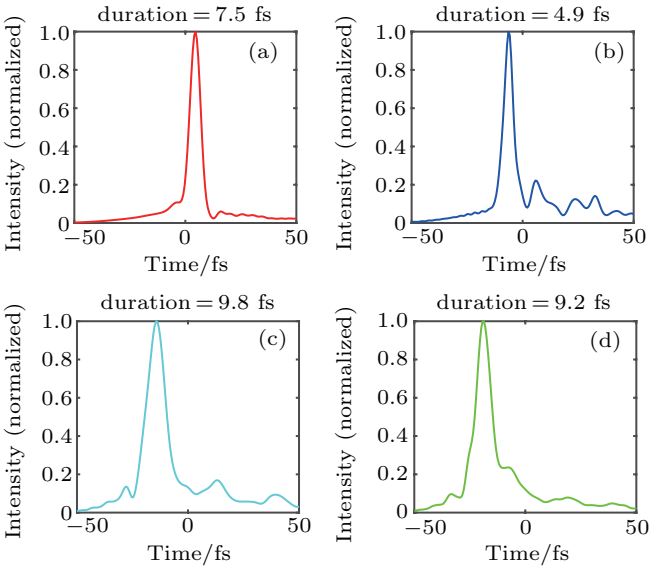


Fig. 11. Temporal power profiles of compressed pulses with different input energy values: (a) 5.0 mJ, (b) 10.0 mJ, (c) 15.0 mJ, and (d) 20.0 mJ. Durations of compressed pulses are 7.5 fs, 4.9 fs, 9.8 fs, and 9.2 fs with GDD compensation of -50 fs^2, -38 fs^2, -38 fs^2, -39 fs^2 shown in panels (a)–(d), while TOD compensation for output pulses is 80 fs^3.

while they vary quadratically with the propagation distance when the initial energy values are 15.0 mJ and 20.0 mJ. This is due to the fact that the energy loss of the pulses propagating in the HCF typically results from the plasma defocusing effect.

Figures 11 and 12 show the temporal power profiles and spatial intensity profiles of the compressed pulses, respectively. Obviously, the temporal power profiles become cleaner with initial energy decreasing, which indicates that the chirp of the output pulses is more difficult to compensate for only by GDD and TOD compensation when the input energy is more than 10.0 mJ. The spot sizes of the spatial intensity profiles of the compressed pulses are greater than those in the other cases for initial energy of 0.5 mJ. In particular, it is evident that the peak intensity and peak power are both stronger than those of other duty cycles when the input energy is 10.0 mJ.

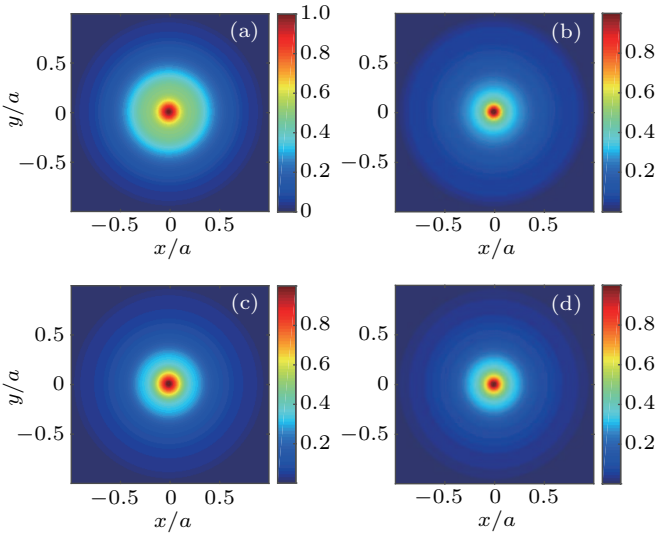


Fig. 12. Normalized spatial intensity profiles of compressed pulses with input energy values ranging from 5.0 mJ to 20.0 mJ, corresponding to scenarios in panels (a)–(d).

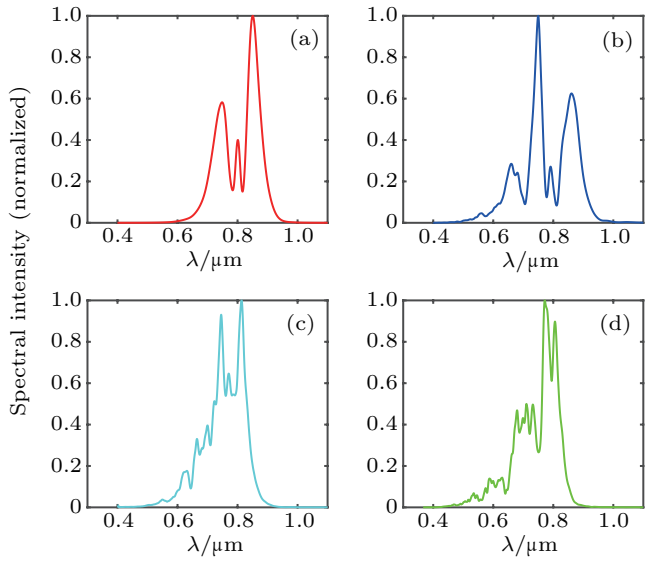


Fig. 13. (a)–(d) Output power spectra of input pulses passing through concentric phase mask with input energy values ranging from 5.0 mJ to 20.0 mJ.

According to the trend of the variation of the output power spectrum of the compressed pulses shown in Fig. 13, the output power spectrum for the input energy of 10.0 mJ is broader than the power spectra for other initial energy values, and a higher peak intensity induces a stronger blue-shift in the power spectrum when the input energy increases. Theoretically, the broader spectrum can be obtained easier by increasing initial energy under the same conditions; however, to reduce the energy loss of pulses during the propagation in the HCF, it is necessary to reduce the pressure of the gas within the HCF at the expense of the narrower spectra for the case of the input pulses of ultra-high energy. Therefore, intense ultrashort pulses can be obtained by using a concentric phase mask under a duty cycle of 0.4. Moreover, if the initial energy increases to 30.0 mJ or more, the energy transmission can be less than 40% and the spatio-temporal splitting is more obvious, which imposes an upper limit on the initial energy.

4. Conclusions

We have numerically studied the dynamic propagation and compression of high-energy input pulses with and without a concentric phase mask in a neon-filled HCF. The results show that 6.5-mJ, 5-fs pulses with more than 65% transmission efficiency can be obtained. The transmission efficiency of the high-energy pulses with the concentric phase mask are considerably higher than without the concentric phase mask. It is found that the peak intensity of the input pulse after the concentric phase mask is less than that without using the concentric phase mask. A decrease in peak intensity of the input pulse results in the reduction of the ionization effect due to plasma generation, which reduces the energy loss of the pulses propagating in the HCF and suppresses the SPM effects producing more high-order chirps. Therefore, the generation of energetic few-cycle pulses by using a concentric phase mask is feasible. The simulation results indicate a robust and efficient scheme to generate intense ultrashort laser pulse sources delivering high-energy chirps and relatively weak chirps. The scheme promises to enhance several existing applications and to enable new applications in the ultrafast science and in extreme nonlinear optics.

References

[1] Zhou J, Peatross J, Murnane M M, Kapteyn H C and Christov I P 1996 *Phys. Rev. Lett.* **76** 752
[2] Krausz F and Ivanov M 2009 *Rev. Mod. Phys.* **81** 163
[3] Zhang W H and Chen L X 2018 *Chin. Opt. Lett.* **16** 030501
[4] Scrinzi A, Ivanov M Y, Kienberger R and Villeneuve D M 2006 *J. Phys. B: At. Mol. Opt. Phys.* **39** R1
[5] Feng X, Gilbertson S, Mashiko H, Wang H, Khan S D, Chini M, Wu Y, Zhao K and Chang Z 2009 *Phys. Rev. Lett.* **103** 183901

[6] Li M, Zhang G Z, Zhao T Q, Ding X and Yao J Q 2017 *Chin. Opt. Lett.* **15** 120202
[7] Li M, Zhang G Z, Zhao T Q, Ding X and Yao J Q 2017 *Chin. Opt. Lett.* **15** 110201
[8] Gopal A, Herzer S, Schmidt A, Singh P, Reinhard A, Ziegler W, Brömmel D, Karmakar A, Gibbon P, Dillner U, May T, Meyer H G and Paulus G G 2013 *Phys. Rev. Lett.* **111** 074802
[9] Geddes G G, Toth C S, Tilborg J V, Esarey E, Schroeder C B, Bruhwiler D, Nieter C, Cary J and Leemans W P 2004 *Nature* **431** 538
[10] Zhong M C, Wang Z Q and Li Y M 2017 *Chin. Opt. Lett.* **15** 051401
[11] Carbajo S, Nanni E A, Wong L J, Moriena G, Keathley P D, Laurent G, Miller R J D and Kartner F X 2016 *Phys. Rev. Accel. Beams* **19** 021303
[12] Wu Y, Cunningham E, Zang H, Li J, Chini M, Wang X, Wang Y, Zhao K and Chang Z 2013 *Appl. Phys. Lett.* **102** 201104
[13] Shirakawa A, Sakane I, Takasaka M and Kobayashi T 1999 *Appl. Phys. Lett.* **74** 2268
[14] Hädrich S, Demmler S, Rothhardt J, Jocher C, Limpert J and Tünnermann A 2011 *Opt. Lett.* **36** 313
[15] Liu H J, Zhao W, Chen G F, Wang Y S, Yu L J, Ruan C and Lu K Q 2004 *Chin. Phys. Lett.* **21** 94
[16] Mourou G, Mironov S, Khazanov E, Sergeev A 2014 *Eur. Phys. J. Spec. Top.* **223** 1181
[17] Lu C H, Tsou Y J, Chen H Y, Chen B H, Cheng Y C, Yang S D, Chen M C, Hsu C C and Kung A H 2014 *Optica* **1** 400
[18] Vuong L T, Lopez-Martens R B, Hauri C P and Gaeta A L 2008 *Opt. Express* **16** 390
[19] Adachi S and Suzuki T 2017 *Opt. Lett.* **42** 1883
[20] Liu Y H, Sun H Y, Ju J J, Tian Y, Bai Y F, Wang C, Wang T J, Liu J S, Chin S L and Li R X 2016 *Chin. Opt. Lett.* **14** 031401
[21] Hädrich S, Klenke A, Hoffmann A, Eidam T, Gottschall T, Rothhardt J, Limpert J and Tünnermann A 2013 *Opt. Lett.* **38** 3866
[22] Nisoli M, Silvestri S D and Svelto O 1996 *Appl. Phys. Lett.* **68** 2793
[23] Jacqmin H, Jullien A, Mercier B, Hanna M, Druon F, Papadopoulos D and Lopez-Martens R 2015 *Opt. Lett.* **40** 709
[24] Böhle F, Kretschmar M, Jullien A, Kovacs M, Miranda M, Romero R, Crespo H, Morgner U, Simon P, Lopez-Martens R and Nagy T 2014 *Laser Phys. Lett.* **11** 095401
[25] Wang D, Leng Y X and Xu Z Z 2012 *Opt. Commun.* **285** 2418
[26] Kang Z, Yuan J H, Li S, Xie S L, Yan B B, Sang X Z and Yu C X 2013 *Chin. Phys. B* **22** 114211
[27] Chen H W, Guo L, Jian A J, Chen S P, Hou J and Lu Q S 2013 *Acta Phys. Sin.* **62** 154207 (in Chinese)
[28] Bohman S, Suda A, Kanai T, Yamaguchi S and Midorikawa K 2010 *Opt. Lett.* **35** 1887
[29] Cardin V, Thire N, Beaulieu S, Wanie V, Legare F and Schmidt B E 2015 *Appl. Phys. Lett.* **107** 181101
[30] Dutin C F, Dubrouil A, Petit S, Mével E, Constant E and Descamps D 2010 *Opt. Lett.* **35** 253
[31] Chen X, Jullien A, Malvache A, Canova L, Borot A, Trisorio A, Durfee C G and Lopez-Martens R 2009 *Opt. Lett.* **34** 1588
[32] Song L W, Li C, Bai Y, Xu R J, Liu P, Li R X and Xu Z Z 2014 *Appl. Phys. B* **115** 93
[33] Carbajo S, Granados E, Schimpf D, Sell A, Hong K H, Moses J and Kärtner F X 2014 *Opt. Lett.* **39** 2487
[34] Wang D, Qiao L L, Zhao R R, Zhao Y and Leng Y X 2017 *Opt. Express* **25** 3083
[35] Fu Y X, Xiong H, Xu H, Yao J P, Zeng B, Chu W, Cheng Y, Xu Z Z, Liu W W and Chin S L 2009 *Opt. Lett.* **34** 3752
[36] Rohwetter P, Queißer M, Stelmaszczyk K, Fechner M and Wöste L 2008 *Phys. Rev. A* **77** 013812
[37] Liu L, Wang C, Cheng Y, Gao H and Liu W W 2011 *J. Phys. B: At. Mol. Opt. Phys.* **44** 215404
[38] Kolesik M and Moloney J V 2004 *Phys. Rev. E* **70** 036604
[39] Andreasen J and Kolesik M 2013 *Phys. Rev. E* **87** 053303
[40] Andreasen J and Kolesik M 2012 *Phys. Rev. E* **86** 036706
[41] Borodin A V, Panov N A, Kosareva O G, Andreeva V A, Esaulkov M N, Makarov V A, Shkurinov A P, Chin S L and Zhang X C 2013 *Opt. Lett.* **38** 1906
[42] Perelomov A M, Popov V S and Terent'ev M V 1966 *Sov. Phys. JETP* **23** 924
[43] Couairon A, Brambilla E, Corti T, Majus D, J Ramírez-Góngora O and Kolesik M 2011 *Eur. Phys. J. Spec. Top.* **199** 5